# Strong Ground Motion and Pulse-Like Velocity Observations in the Near-Fault Region of the 2018 $M_w$ 6.4 Hualien, Taiwan, Earthquake

by Chun-Hsiang Kuo, Jyun-Yan Huang, Che-Min Lin, Ting-Yu Hsu, Shu-Hsien Chao, and Kuo-Liang Wen

## ABSTRACT

The maximum observed peak ground acceleration (PGA) and peak ground velocity (PGV) at various stations during the 2018 Hualien, Taiwan earthquake were 594 Gal and 146 cm/s, respectively. Pulse-like velocities were observed at all stations within a distance of 4 km from the Milun fault. The horizontal spectral accelerations of the pulse-like records indicated two obvious amplifications at periods of roughly 1 and 2 s. Natural frequencies of 0.8–1.5 Hz were observed in the region near the Milun fault using microtremor measurements. The spectral acceleration peak at periods of roughly 2 s is mostly seen in the east–west direction, indicating a typical fault-normal seismic radiation from the fault rupture. Consequently, we contend that the amplifications of spectral acceleration at approximately 1 and 2 s were caused by site amplification and the rupture front, respectively. The site amplification at approximately 1 s may have been one reason for the collapse of medium-rise buildings during this earthquake. Evident soil nonlinearity resulted in smaller horizontal than vertical PGA at many stations in the near-fault region.

## INTRODUCTION

A destructive earthquake with a moment magnitude ($M_w$) of 6.4 occurred offshore to the north of Hualien City on 6 February 2018. It left 17 fatalities, 285 injuries, and more than 175 damaged buildings and two damaged bridges across faults. An apparent slip of the Milun fault was observed during the earthquake, although the epicenter was roughly 12.5 km offshore of the surface fault trace. According to the report released by the Central Weather Bureau (CWB), the epicenter was located at 121.7297° E and 24.1007° N (Fig. 1), the focal depth was 6.31 km, and the magnitude ($M_w$) was 6.2. The CWB calculated the focal mechanism using the centroid moment tensor solution and broadband seismic data obtained in Taiwan. The strike/dip/rake of the two obtained nodal planes were 216°/56°/26° and 111°/69°/144. The U.S. Geological Survey (USGS) and Global Centroid Moment Tensor (CMT) project calculated similar mechanisms but a larger magnitude

of 6.4. The Central Geological Survey (CGS) in Taiwan found clear left-lateral slips along the Milun and Lingding faults after the Hualien earthquake according to both Global Positioning System observations and field investigations (Central Geological Survey [CGS], 2018). The real fault plane thus had to have the strike in a nearly north–south direction; that is, 216°/56°/26°.
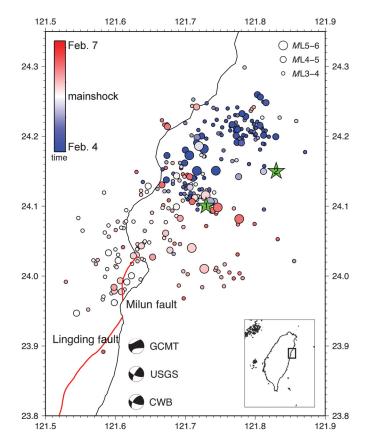
Several days before the mainshock, seismicity in the near-source region was increased. The largest foreshock ($M_w$ 6.1) occurred 50 hrs before the mainshock. The seismicity of the Hualien earthquake exhibited an obvious migration before and after the mainshock, as illustrated in Figure 1.

Stations located along the Milun fault observed pulse-like velocities, which are believed to be the most destructive seismic waves for medium- to high-rise buildings because of their large amplitude and long-period pulses. (Heaton et al., 1995; Somerville et al., 1997; Shahi and Baker, 2014). Four medium-rise buildings (7–12 floors) constructed from the 1970s to 1990s and located very near the Milun fault (distance < 1 km) collapsed during this earthquake (National Center for Research on Earthquake Engineering [NCREE], 2018). The seismic waves exhibiting pulse-like velocity may have exerted a large seismic force on these collapsed buildings.

The site effect always plays a major role in determining the characteristics of strong ground motions. $V_{S30}$, the average $S$-wave velocity in the top 30 m, has been widely used in ground-motion prediction equations (GMPEs) and building codes (Building Seismic Safe Council [BSSC], 1997; Abrahamson and Silva, 2008; Chiou and Youngs, 2008). Otherwise, the dominant frequency of a site can usually be determined using the microtremor horizontal-to-vertical spectral ratio (MHVSR; Nakamura, 1989; Parolai et al., 2001; Sánchez-Sesma et al., 2011; Kuo et al., 2015). In this article, the site characteristics of Hualien City and the nearby region were determined and discussed to understand the strong motions of the large Hualien earthquake.

## STRONG GROUND MOTION OBSERVATION

The CWB has installed more than 800 free-field strong-motion stations throughout Taiwan, and the data is available

▲ **Figure 1.** Spatial and temporal distribution of foreshocks, mainshock, and aftershocks from 4 to 7 February 2018. The mainshock (indicated as number 1) and the largest foreshock (indicated as number 2) are marked with green stars. The lower right inset indicates Taiwan island and the frame (black rectangle) of this figure.

via the geophysical database management system (GDMS) (Shin *et al.*, 2013). The National Center for Research on Earthquake Engineering (NCREE) recently constructed the seismic array of NCREE in Taiwan (SANTA), which is a network of 37 real-time data collection stations equipped with strong motion and broadband sensors. The NCREE has also constructed an onsite earthquake early warning system (NEEWS). The NEEWS performed relatively well in recent damaging earthquakes such as the 2016 Meinong and 2018 Haulien earthquakes (Hsu *et al.*, 2016, 2018). In addition, a regional EEW system is provided by the CWB (Hsiao *et al.*, 2009), and the National Taiwan University group reports on-site warning in many research works (Wu *et al.*, 2016, 2018). This study combined data from the 270 stations in the network of the CWB and the 37 stations in the network of the NCREE (SANTA and NEEWS) to analyze the strong ground motion characteristics evident during the Hualien earthquake.
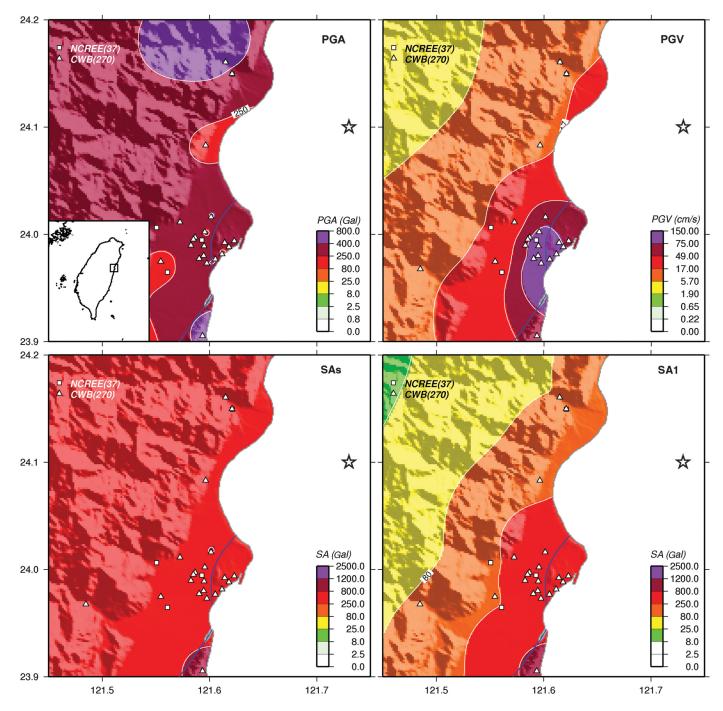
The maximum observed peak ground acceleration (PGA) was 594 Gal (north–south component) at the HWA057 station with an epicentral distance of 12.6 km; the maximum observed peak ground velocity (PGV) was 146 cm/s in east–west component at the HWA014 station with an epicentral distance

of 19.1 km. The shake map of the PGA, PGV, and spectral accelerations of 0.3 (SA0.3) and 1 s (SA1.0) are depicted in Figure 2. Taiwan determines the official intensity of earthquakes using only PGA. According to that scale, an intensity level of 7 (PGA > 400 Gal), the highest level on the CWB's scale, was recorded at five stations. These stations are sporadically distributed from north to south and across a range of 60 km. We also adopted another nonofficial intensity scale that uses comparable PGV (Wu *et al.*, 2003) and then determined that an intensity level of 7 (PGV > 75 cm/s) was recorded at 10 stations, all of which were located along the Milun fault. The fragmentary distribution of the value of the short-period response acceleration (SA)0.3 between 800 and 1200 Gal was similar to that of the PGA. However, the distribution pattern of the long-period response acceleration SA1.0 was similar to that of the PGV. High PGV and/or SA1.0 along the Milun fault indicated that Hualien City suffered strong shaking at a period of 1 s, which may have been the major cause of the collapse of the four medium-rise buildings.

The strong ground motions recorded were compared with the ground motions estimated using the Chao *et al.* (2017, hereafter, Chao17) GMPE, which was developed using only Taiwan data; the comparison is presented in Figure 3. Because of the lack of a reliable finite-fault model, we used the hypocentral distances of the stations for most of the intensity measures. For the near-fault stations, we directly used the distance from the stations to the Milun fault as the shortest distance to the rupture (Rrup), because clear surface ruptures along the fault were observed after the mainshock (Lee *et al.*, 2018). Figure 3 depicts the comparison in terms of horizontal PGA, SA1.0, and SA3.0, respectively. The GMPEs are plotted using $V_{S30}$ of 240, 360, and 760 m/s for various site amplifications. The observed horizontal motions were converted into their RotD50 components, which is the median ground motion over all horizontal orientations. We were particularly interested in the near-fault results (open circles) in this case. The estimated and observed ground motions were similar for short periods (PGA), but the ground motions estimated using the GMPE were underestimated for long periods (SA1.0 and SA3.0). The Chao17 GMPE still does not consider long-period ground motions caused by the forward-directivity effect, which would account for the obvious underestimation in the near-fault region.
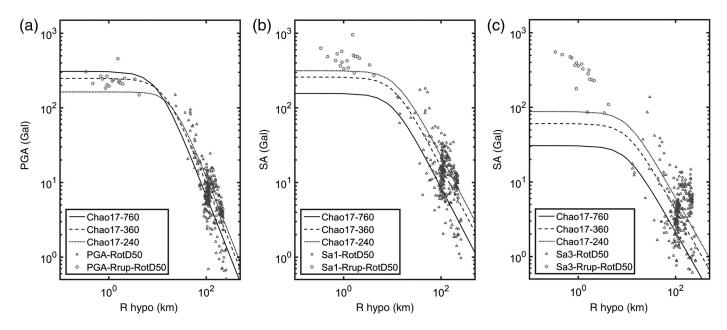
## SEISMIC SITE CONDITIONS

Seismic site conditions in the near-fault region were investigated to understand the site effect and to further determine the strong ground motion behavior. Especially at the near-surface, $S$-wave velocity ($V_S$) has a major influence on seismic-wave amplifications. Various $V_S$ values and thicknesses of layers can amplify seismic waves at specific frequencies differently. $V_{S30}$ is a continuous number that relates to the stiffness of ground layers. For the sake of convenience and generality, $V_{S30}$ has been widely used to account for site amplifications in various approaches to strong ground motion prediction. In
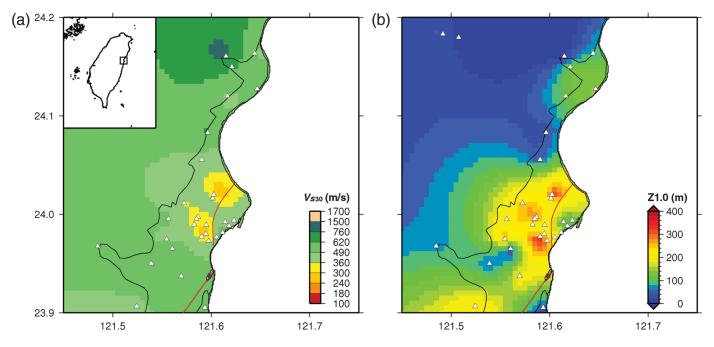
▲ **Figure 2.** Spatial distribution of intensity measures (peak ground acceleration [PGA], peak ground velocity [PGV], spectral accelerations [SAs], and SA1) in the Hualien region during the mainshock. The inset in lower left of the PGA map indicates Taiwan island and the frame (black rectangle) of this figure.

recent years, a new site parameter was introduced in advanced GMPEs in the Next Generation Attenuation (NGA) projects to account for sedimentary depth (i.e., Z1.0; Abrahamson et al., 2014; Boore et al., 2014; Chiou and Youngs, 2014) and to increase the accuracy of ground motion predictions. Z1.0 is the depth from the surface to the top of the layer with $V_S > 1$ km/s. Combining $V_{S30}$ and Z1.0 enabled us to consider both velocity and depth of soft sediments by using GMPEs.

Kuo et al. (2017) obtained $V_{S30}$ data based on the $V_S$ profiles logged at most of the free-field strong-motion stations (Kuo et al., 2012) and then used estimations of $V_{S30}$ values (Lin et al., 2014; Kwok et al., 2018) to supplement those without logged data. Z1.0 data from the same network were obtained from logged $V_S$ profiles, microtremor arrays (Kuo et al., 2016), receiver functions, or MHVSR inversions. We extracted the site parameters in the Hualien area to illustrate the distributions depicted in Figure 4. The white triangles
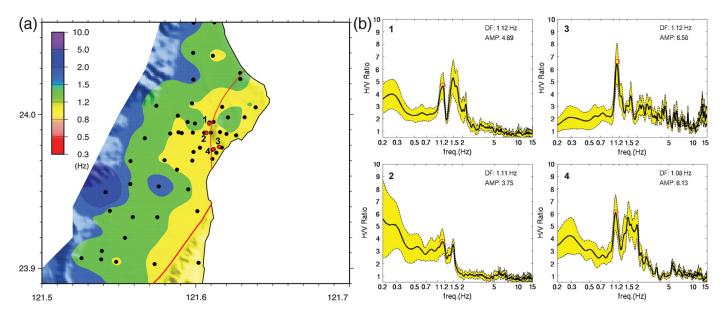
▲ **Figure 3.** Comparison of observed strong motions and those estimated from the Chao *et al.* (2017; referred to as Chao17) ground-motion prediction equation (GMPE), assuming $V_{S30} = 240$, 360, and 760 m/s: (a) PGA, (b) spectral acceleration at 1 s (SA1), and (c) spectral acceleration at 3 s (SA3). Rrup was used to find the circles and hypocentral distance for the triangles.



▲ **Figure 4.** Distributions of (a) $V_{S30}$ and (b) Z1.0 in the Hualien region. The inset in upper left of the $V_{S30}$ map indicates Taiwan island and the frame (black rectangle) of this figure.

represent stations with parameters; other grids were interpolated into 0.3 arc-min (∼0.5 km) using block average method by Generic Mapping Tools (Wessel and Smith, 1998). The $V_{S30}$ map indicates that the $V_{S30}$ in the Hualien area is mostly between 360 and 760 m/s and belongs to site class C; however, part of Hualien City is site class D with a $V_{S30}$ between 240 and 360 m/s (BSSC, 1997). Borehole data indicate that the

shallow layers are composed of sand, clay, and gravel in this region. The soft soils are primarily distributed to the west of the Milun fault. The Z1.0 map depicts the presence of a sedimentary thickness of roughly 300 m to the west of the Milun fault, whereas the eastern terrace has a thickness of approximately 100–200 m. To the east of the Milun fault, there is a terrace with higher topography and velocity. To the east of
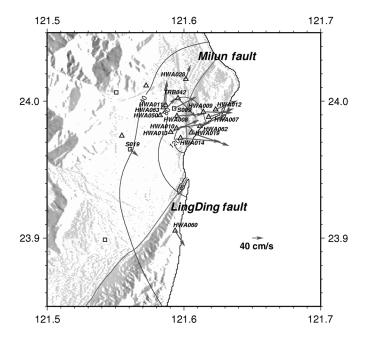
▲ **Figure 5.** Microtremor horizontal-to-vertical spectral ratio (MHVSR) results in the Hualien region: (a) distribution of dominant frequency; (b) MHVSR at the four sites indicated in (a).

Milun fault is Milun formation (Pleistocene) and to the west of Milun fault is Alluvium (Holocene) (Chen *et al.*, 2010), so a maximum depth difference of ∼200 m across Milun fault is likely due to different geological conditions.
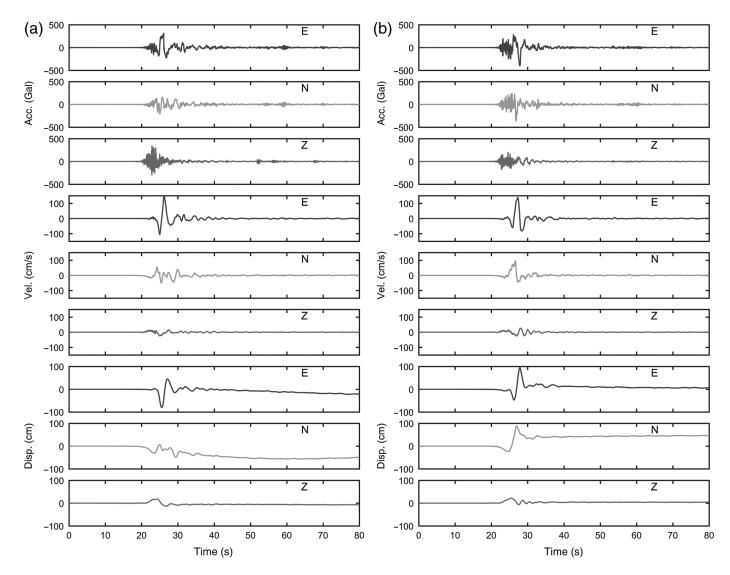
Another well-known approach to understand site effects is microtremor measurement. Figure 5 depicts contours of the dominant frequencies of MHVSRs in the Hualien area. The black dots indicate single-station measurements and other grids were interpolated. We interpret the resonant frequency of *S*-wave amplification should be similar to that of MHVSR, because clear peaks (namely for sufficiently high-impedance contrast) can be seen in most of the MHVSRs in this region. The predominant frequencies in downtown Hualien are 0.8–1.5 Hz (yellow and green), changing to 1.2–1.5 Hz (green) to the west and further increasing to higher than 1.5 Hz in the mountain range (blue). The locations of the microtremor measurements are different from those used in Figure 4, and thus the distribution of predominant frequency (Fig. 5a) is not so similar to those of $V_{S30}$ and Z1.0 (Fig. 4). Three MHVSRs near the collapsed buildings (red dots; numbers 1, 2, and 4) are shown as well as an additional MHVSR for comparison (red dot; number 3). All of them exhibit an obvious peak at 1 Hz, which indicates a uniform predominant frequency in the area (yellow).

## NEAR-FAULT GROUND MOTIONS

Typical near-fault strong ground motions were recorded during the $M_w$ 6.4 Hualien mainshock at all stations on both sides of the Milun fault within 4 km, which is the distance between the S019 station and the Milun fault. Somerville *et al.* (1997) contended that pulse-like velocities are usually observed in fault-normal and fault-parallel directions because of the *S*-wave radiation and fling effects in cases of strike-slip faulting.

Kawase (1996) used numerical simulation to determine that the high amplitudes of the pulse-like velocities of the Kobe, Japan, earthquake were caused by the basin-edge effect to the pulse-like input. We adopted the pulse indicator method proposed by Shahi and Baker (2014) to identify the distribution of pulse-like velocities and maximum pulse direction for each station. Figure 6 displays the 17 stations having pulse-like velocities and the maximum pulse directions (arrows) and PGV contours during the mainshock. The results clearly indicate



▲ **Figure 6.** Locations of 17 stations that recorded pulse-like velocities and the maximum pulse direction. Contours are the PGV distribution.
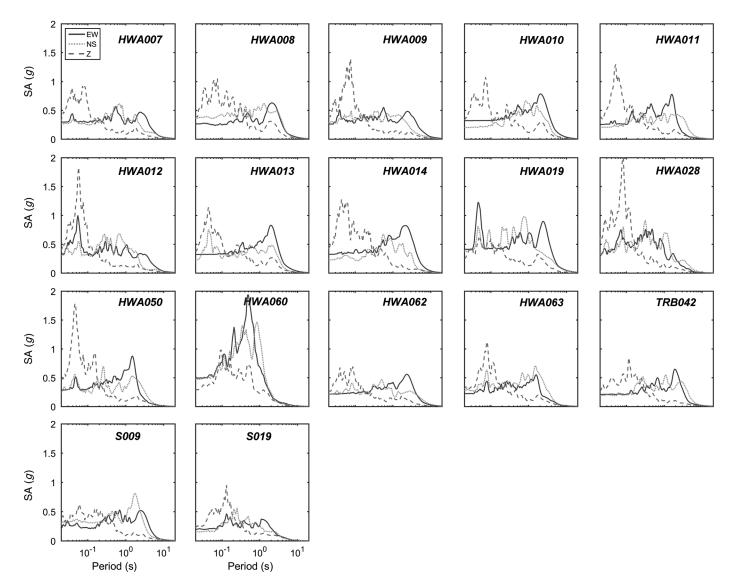
▲ **Figure 7.** Strong-motion waveforms after baseline correction in terms of acceleration, velocity, and displacement at stations (a) HWA014 and (b) HWA019.

that pulse-like velocities were observed on both sides of the Milun fault and that the maximum pulses were mostly in the fault-normal direction (east–west), especially near the southern portion of the Milun fault. In this case, the pulse-like velocities were observed at stations along the Milun fault with epicentral distances from 15.5 km (HWA028) to 25.4 km (HWA060). The PGV contour demonstrates that the maximum PGV was larger than 120 cm/s and was observed at the southern end of the Milun fault.

We thus know that the seismic site conditions ($V_{S30}$ and Z1.0) at the left and right sides of the Milun fault are different; however, pulse-like velocities were observed on both sides and were strongest mostly in the fault-normal direction. Because most stations at locations with various site conditions recorded very similar strong motions, that is, pulse-like velocities in the same direction (east–west), we therefore speculated that the pulse-like velocities recorded in the mainshock were not caused by the basin-edge effect.

The largest velocities and coseismic displacements occurred at stations HWA019 and HWA014, which are located to the east and west of the south end of the Milun fault, respectively. We removed the baseline drifts from the velocity traces, and the resultant velocities and displacements are depicted in Figure 7. The coseismic displacements indicated slight movements of roughly 0.5 m to the north and south at the east and west sides of the Milun fault, indicating slipping to the left during the mainshock.

The three-component spectral accelerations at the 17 stations with velocity pulses were then calculated and are displayed in Figure 8. The 17 stations included the 15 Taiwan strong motion instrumentation program (TSMIP) stations and two NEEWS stations (S009 and S019). Distinct peaks of spectral accelerations at periods of approximately 2 s were evident at most stations, especially from the east–west (fault-normal) direction. The long-period peaks of spectral accelerations were identified as pulse-like waves (Shahi and Baker, 2014);
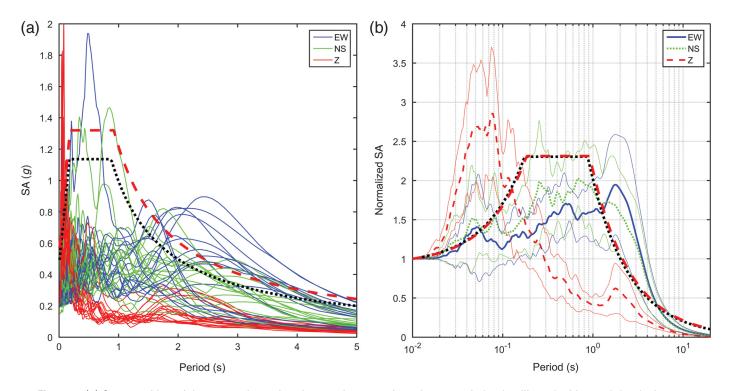
▲ **Figure 8.** Three components of spectral accelerations at the 17 stations that recorded pulse-like velocities. Solid, dotted, and dashed curves represent the east–west, north–south, and vertical components, respectively.
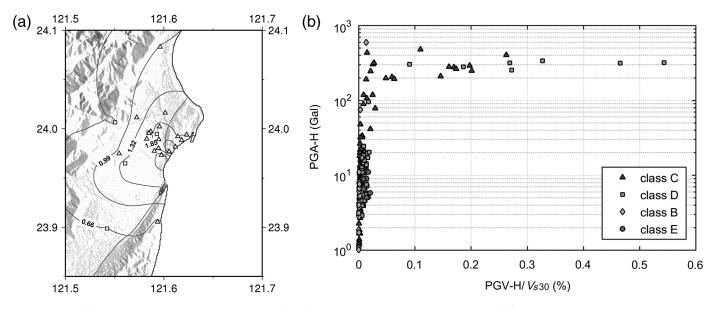
however, this revealed the problem that long-period accelerations go beyond the design and maximum consideration spectra. The spectral accelerations of the 17 stations with velocity pulses were superimposed with the 475 yr and 2500 yr design spectra (Construction and Planning Agency [CPA], 2011), as displayed in Figure 9a. Although both the design spectra considered the maximum site amplification and near-fault factors for conservative comparison, the spectral accelerations at periods longer than 1.5 s still exceeded the most conservative design spectra for this region. Figure 9b indicates the average result of the normalized spectral accelerations at the 16 stations with velocity pulses. Station HWA060 was not included because it is located near the Lingding fault but not the Milun fault. The closest stations to the collapsed medium-rise buildings, HWA008 and HWA019 (Fig. 8), recorded an obvious spectral acceleration peak at roughly 1 s from the north–south component and another peak at approximately

2 s from the east–west component. On the basis of microtremor analysis, we presume that the 1 s peak was also amplified by local site effect and that the 2 s peak in the fault-normal direction might have been caused by the asperity, forward directivity amplification, and radiation pattern of the shear dislocation on the fault.

## SOIL NONLINEARITY

The strong ground motions recorded at several stations in Hualien City exhibited larger vertical than horizontal PGA; however, the horizontal PGV was still larger than the vertical PGV. Larger vertical-to-horizontal ratios (V/H) of short-period seismic waves are usually observed in the near-fault region during large events (e.g., Bozorgnia and Campbell, 2016). This phenomenon is more obvious at soft soil sites than at stiff soil sites, and thus the major reason for its occurrence is

▲ **Figure 9.** (a) Superposition of the spectral accelerations at the 17 stations that recorded pulse-like velocities and the design spectra (black and red dotted lines). (b) Average three-component spectral accelerations at 16 stations.



▲ **Figure 10.** (a) Distribution of vertical-to-horizontal (V/H) ratios of PGA in the Hualien region. (b) PGA–PGV/$V_{S30}$ relationship derived from strong motions during the Hualien earthquake.

believed to be soil nonlinearity during near-fault strong shaking. The V/H of PGA at each station in this event was calculated, and the contours of V/H are plotted in Figure 10a. The horizontal PGA was rotated to RotD50. The V/H at downtown Hualien was higher than 1.3 and at the southern portion of the Milun fault was even higher than 1.6.

To further assess soil nonlinearity during the earthquake, we used the PGA–PGV/$V_{S30}$ relationship as a proxy for the stress–strain relationship (Idriss, 2011; Chandra *et al.*, 2016; Guéguen, 2016). We divided stations into four groups according to the site classification (BSSC, 1997), and the result is presented in Figure 10b. Large strain was evident at several class C and D stations which are located in Hualien City. We therefore speculated that soil nonlinearity reduced the strength of high-frequency horizontal ground motions as well as damage to low-rise buildings in downtown Hualien.

**Table 1**
**$V_{S30}$ and Basic Ground-Motion Intensity Measures of 17 Stations that Recorded Pulse-Like Velocities**

| Station Code | $V_{S30}$ (m/s) | PGA (Gal) | PGV (cm/s) | V/H$_{PGA}$ | $R_{hypo}$ (km) | $R_{rup}$ (km) |
|---|---|---|---|---|---|---|
| HWA007 | 379* | 289.02 | 74.85 | 1.12 | 17.6 | 1.7 |
| HWA008 | 297.03 | 336.48 | 97.19 | 1.25 | 19.0 | 0.7 |
| HWA009 | 461* | 317.55 | 80.12 | 1.34 | 17.5 | 1.3 |
| HWA010 | 249.68 | 313.98 | 116.25 | 1.16 | 19.7 | 0.7 |
| HWA011 | 360.84 | 327.11 | 72.57 | 1.48 | 19.1 | 1.6 |
| HWA012 | 409.78 | 338.37 | 65.98 | 1.35 | 16.8 | 2.1 |
| HWA013 | 336.76 | 323.62 | 90.53 | 1.41 | 20.2 | 1.2 |
| HWA014 | 279.96 | 348.27 | 146.46 | 1.87 | 20.1 | 0.5 |
| HWA019 | 503.52 | 403.00 | 138.39 | 0.70 | 19.3 | 0.3 |
| HWA028 | 404.91 | 414.84 | 68.66 | 1.56 | 16.7 | 0.9 |
| HWA050 | 343* | 336.94 | 64.08 | 1.61 | 19.9 | 1.9 |
| HWA060 | 556* | 477.89 | 61.15 | 0.62 | 26.2 | 1.5 |
| HWA062 | 605.69 | 213.80 | 88.32 | 1.09 | 18.5 | 1.0 |
| HWA063 | 289* | 253.40 | 78.68 | 1.18 | 19.3 | 1.7 |
| TRB042 | – | 219.17 | 80.10 | 1.19 | 18.1 | 0.9 |
| S009 | – | 304.97 | 94.72 | 0.93 | 18.8 | 0.9 |
| S019 | 579.60 | 219.03 | 36.83 | 1.47 | 23.2 | 4.2 |

PGA, peak ground acceleration; PGV, peak ground velocity; V/H, vertical-to-horizontal.
*Estimated $V_{S30}$ from Kwok *et al.* (2018) and Lin *et al.* (2014).

## DISCUSSION AND CONCLUSIONS

The $V_{S30}$ and basic intensity measures of the 17 stations observed pulse-like velocities are listed in Table 1. The PGVs at HWA014 and HWA019 stations were 146 and 138 cm/s (Fig. 7), respectively, which are relatively large for an earthquake with magnitude of 6.4; however, the PGAs were 0.3*g* and 0.4*g*, which were not unexpected values. Figure 9b exhibits mean normalized spectral accelerations from the recordings with pulse-like velocities. The maximum SAs of east–west and north–south are at approximately 2 and 1 s, respectively.

With the benefit of data from high-density free-field strong-motion stations, we were able to analyze the Hualien earthquake by using a dozen near-field recordings. The Milun fault, which passes through Hualien City from the north to the south, exhibited obvious strike-slip faulting during this event, and thus all 16 stations on both sides of the fault within 4 km of the fault recorded a large amplitude and long-period velocity pulse. The major disaster caused by this event—the collapse of four medium-rise buildings—may also be influenced by site amplifications at a period of approximately 1 s. The other peak in spectral acceleration occurred at a longer period of roughly 2 s in a fault-normal direction (east–west) and was thus presumably generated by the asperity, forward-directivity amplification, and the seismic radiation of the shear dislocation on the fault. Smaller horizontal than vertical PGA was observed at several stations near the Milun fault, indicating strong soil nonlinearity in this region during the earthquake. We speculated that this was one reason that the low-rise buildings avoided serious damage during this earthquake.

## DATA AND RESOURCES

The strong-motion accelerations of the Taiwan strong motion instrumentation program (TSMIP) can be downloaded from the geophysical database management system (GDMS) website (http://gdms.cwb.gov.tw/index.php, last accessed June 2018). The strong-motion accelerations of seismic array of NCREE in Taiwan (SANTA) and the earthquake early warning system (NEEWS) can be acquired by contacting the authors. The Chinese and English reports released by the National Center for Research on Earthquake Engineering (NCREE) can be found on their website (http://www.ncree.org/Ncree.aspx?id=17, last accessed June 2018). The focal mechanisms are attributable to the Central Weather Bureau (CWB) (https://www.cwb.gov.tw/V7/earthquake/rtd_eq.htm, last accessed June 2018), U.S. Geological Survey (USGS) (https://earthquake.usgs.gov/earthquakes/eventpage/us1000chhc#executive, last accessed June 2018), and Global Centroid Moment Tensor (CMT) (http://www.globalcmt.org/CMTsearch.html, last accessed June 2018).

## REFERENCES

Abrahamson, N. A., and W. J. Silva (2008). Summary of the Abrahamson & Silva NGA ground motion relations, *Earthq. Spectra* **24,** 67–97.

Abrahamson, N. A., W. J. Silva, and R. Kamai (2014). Summary of the ASK14 ground motion relation for active crustal region, *Earthq. Spectra* **30,** 1025–1055.

Boore, D. M., J. P. Stewart, E. Seyhan, and G. A. Atkinson (2014). NGA-West2 equations for predicting PGA, PGV, and 5% damped PSA for shallow crustal earthquakes, *Earthq. Spectra* **30,** 1057–1085.

Bozorgnia, Y., and K. W. Campbell (2016). Ground motion model for the vertical-to-horizontal (V/H) ratios of PGA, PGV, and response spectra, *Earthq. Spectra* **32,** 951–978.

Building Seismic Safe Council (BSSC) (1997). NEHRP recommended provisions for seismic regulations for new buildings and other structures, 1997 Edition, Part 1: Provisions and Part 2: Commentary, Building Seismic Safe Council for the Federal Emergency Management Agency, *Rept. No. FEMA 302 and 303*, Washington, D.C.

Central Geological Survey (CGS) (2018). Geology survey report of the 2018.02.06 Hualien earthquake, *Central Geology Survey*, Ministry of Economic Affairs, Taipei, Taiwan (in Chinese).

Chandra, J., P. Guéguen, and L. F. Conilla (2016). PGA-PGV/Vs considered as a stress-strain proxy for predicting nonlinear soil response, *Soil Dynam. Earthq. Eng.* **85,** 146–160.

Chao, S. H., Y. H. Chen, C. C. Hsu, and P. S. Lin (2017). Development of horizontal Taiwan ground motion model for crustal earthquake and subduction earthquake, *Technical Report of National Center for Research on Earthquake Engineering, NCREE-17-009*, 228 pp.

Chen, W. S., Y. Wang, C. N. Yang, and C. C. Barry Yang (2010). Explanatory text for the geologic map of Taiwan in scale 1:50000 - Hualien, *Central Geological Survey*, MOEA, Taipei, Taiwan (in Chinese).

Chiou, B. S.-J., and R. R. Youngs (2008). An NGA model for the average horizontal component of peak ground motion and response spectra, *Earthq. Spectra* **24,** 173–215.

Chiou, B. S.-J., and R. R. Youngs (2014). Update of the Chiou and Youngs NGA model for the average horizontal component of peak ground motion and response spectra, *Earthq. Spectra* **30,** 1117–1153.

Construction and Planning Agency (CPA) (2011). *Seismic Design Code and Commentary for Buildings*, 2011 Ed., Construction and Planning Agency, Ministry of the Interior, Taipei, Taiwan (in Chinese).

Guéguen, P. (2016). Predicting nonlinear site response using spectral acceleration vs PGV/Vs30: A case history using the Volvi-test site, *Pure Appl. Geophys.* **173,** 2047–2063.

Heaton, T. H., J. F. Hall, D. J. Wald, and M. W. Halling (1995). Response of high-rise and base-isolated buildings to hypothetical $M_w$ 7.0 blind thrust earthquake, *Science* **267,** 206–211.

Hsiao, N. C., Y. M. Wu, T. C. Shin, L. Zhao, and T. L. Teng (2009). Development of earthquake early warning system in Taiwan, *Geophys. Res. Lett.* **36,** L00B02, doi: 10.1029/2008GL036596.

Hsu, T. Y., P. Y. Lin, H. H. Wang, H. W. Chiang, Y. W. Chang, C. H. Kuo, C. M. Lin, and K. L. Wen (2018). Comparing the Performance of the NEEWS Earthquake Early Warning System Against the CWB System During the 6 February 2018 $M_w$ 6.2 Hualien earthquake, *Geophys. Res. Lett.* **45,** doi: 10.1029/2018GL078079.

Hsu, T. Y., H. H. Wang, P. Y. Lin, C. M. Lin, C. H. Kuo, and K. L. Wen (2016). Performance of the NCREE's on-site warning system during the 5 February 2016 $M_w$ 6.53 Meinong Earthquake, *Geophys. Res. Lett.* **43,** 8954–8959.

Idriss, I. M. (2011). Use of $V_{S30}$ to represent local site condition, *Proc. of the 4th IASPEI/IAEE international symposium, effects of source geology on seismic motion*, U.C. Santa Barbara, California, 23–26 August.

Kawase, H. (1996). The cause of the damage belt in Kobe: "The Basin-Edge Effect," constructive interference of the direct *S*-wave with the basin-induced diffracted/Rayleigh waves, *Seismol. Res. Lett.* **67,** 25–34.

Kuo, C. H., C. T. Chen, C. M. Lin, K. L. Wen, J. Y. Huang, and S. C. Chang (2016). *S*-wave velocity structure and site effect parameters derived by microtremor arrays in the western plain of Taiwan, *J. Asian Earth Sci.* **128,** 27–41.

Kuo, C. H., C. M. Lin, S. C. Chang, K. L. Wen, and H. H. Hsieh (2017). Site database for Taiwan strong motion stations, *Technical Report of National Center for Research on Earthquake Engineering, NCREE-17-004*, 80 pp.

Kuo, C. H., K. L. Wen, H. H. Hsieh, C. M. Lin, T. M. Chang, and K. W. Kuo (2012). Site classification and $V_{S30}$ estimation of free-field TSMIP stations using the logging data of EGDT, *Eng. Geol.* **129/130,** 68–75.

Kuo, C. H., K. L. Wen, C. M. Lin, S. Wen, and J. Y. Huang (2015). Investigating near surface *S*-wave velocity properties by ambient noise in southwestern Taiwan, *Terr. Atmos. Ocean. Sci.* **26,** 205–211.

Kwok, O. L. A., J. P. Stewart, D. Y. Kwak, and P. L. Sun (2018). Taiwan-specific model for $V_{S30}$ prediction considering between-proxy correlations, *Earthq. Spectra.* doi: 10.1193/061217EQS113M (in press).

Lee, S. J., T. C. Lin, T. Y. Liu, and T. P. Wong (2018). Fault-to-fault jumping rupture of the 2018 $M_w$ 6.4 Hualien earthquake in eastern Taiwan, *Seismol. Res. Lett.* doi: 10.1785/0220180182.

Lin, C. M., K. L. Wen, C. H. Kuo, and C. Y. Lin (2014). *S*-wave velocity model of Taipei Basin, *The 5th Asia Conference on Earthquake Engineering*, Taipei, Taiwan, 16–18 October.

Nakamura, Y. (1989). A method for dynamic characteristics estimation of subsurface using microtremor on the ground surface, *Q. Rep. Railway Tech. Res. Inst.* **30,** 25–33.

National Center for Research on Earthquake Engineering (NCREE) (2018). *A Summary of 2018.02.06 Hualien Earthquake, Version 8*, National Center for Research on Earthquake Engineering, Taipei, Taiwan (in Chinese).

Parolai, S., P. Bormann, and C. Milkereit (2001). Assessment of the nature frequency of the sedimentary cover in the cologne area (Germany) using noise measurement, *J. Earthq. Eng.* **5,** 541–564.

Sánchez-Sesma, F. J., M. Rodriguez, U. Iturrarán-Viveros, F. Luzón, M. Campillo, L. Margerin, A. García-Jerez, M. Suarez, M. A. Santoyo, and A. Rodríguez-Castellanos (2011). A theory for microtremor H/V spectral ratio: Application for layered medium, *Geophys. J. Int.* **186,** 221–225.

Shahi, S. K., and J. W. Baker (2014). An efficient algorithm to identify strong-velocity pulse in multicomponent ground motions, *Bull. Seismol. Soc. Am.* **104,** 2456–2466.

Shin, T. C., C. H. Chang, H. C. Pu, H. W. Lin, and P. L. Lu (2013). The geophysical database management system in Taiwan, *Terr. Atmos. Ocean. Sci.* **24,** 11–18.

Somerville, P. G., N. F. Smith, R. W. Graves, and N. A. Abrahamson (1997). Modification of empirical strong ground motion attenuation relations to include the amplitude and duration effects of rupture directivity, *Seismol. Res. Lett.* **68,** 199–222.

Wessel, P., and W. H. F. Smith (1998). New, improved version of the generic mapping tools released, *Eos Trans. AGU* **79,** 579.

Wu, Y. M., W. T. Liang, H. Mittal, W. A. Chao, C. H. Lin, B. S. Huang, and C. M. Lin (2016). Performance of a low-cost earthquake early warning system (*P*-alert) during the 2016 $M_L$ 6.4 Meinong (Taiwan) earthquake, *Seismol. Res. Lett.* **87,** no. 5, 1050–1059.

Wu, Y. M., H. Mittal, T. C. Huang, B. M. Yang, J. C. Jan, and S. K. Chen (2018). Performance of a low-cost earthquake early warning system

(P-alert) and shake map production during the 2018 $M_w$ 6.4 Hualien (Taiwan) earthquake, *Seismol. Res. Lett.* doi: 10.1785/0220180170.

Wu, Y. M., T. L. Teng, T. C. Shin, and N. C. Hsiao (2003). Relationship between peak ground acceleration, peak ground velocity, and intensity in Taiwan, *Bull. Seismol. Soc. Am.* **91,** 1218–1228.

*Chun-Hsiang Kuo*
*Jyun-Yan Huang*
*Che-Min Lin*
*Shu-Hsien Chao*
*National Center for Research on Earthquake Engineering*
*No. 200, Section 3, Xinhai Roadz*
*Taipei 10668, Taiwan*
*chkuo@ncree.narl.org.tw*
*jyhuang@ncree.narl.org.tw*
*cmlin@ncree.narl.org.tw*
*shchao@ncree.narl.org.tw*

*Ting-Yu Hsu*
*Department of Civil and Construction Engineering*
*National Taiwan University of Science and Technology*
*No. 43, Section 4, Keelung Road*
*Taipei 10607, Taiwan*
*tyhsu@mail.ntust.edu.tw*

*Kuo-Liang Wen*
*Department of Earth Sciences*
*National Central University*
*No. 300, Zhongda Road*
*Taoyuan City 32001, Taiwan*
*wenkl@cc.ncu.edu.tw*